Original Article

Metallurgical and electrochemical characterization of contemporary silver-based soldering alloys

Argyro Ntasi[a]; Youssef Al Jabbari[b]; Wolf Dieter Mueller[c]; George Eliades[d]; Spiros Zinelis[e]

ABSTRACT

Objective: To investigate the microstructure, hardness, and electrochemical behavior of four contemporary Ag-based soldering alloys used for manufacturing orthodontic appliances.

Materials and Methods: The Ag-based alloys tested were Dentaurum Universal Silver Solder (DEN), Orthodontic Solders (LEO), Ortho Dental Universal Solder (NOB), and Silver Solder (ORT). Five disk-shaped specimens were produced for each alloy, and after metallographic preparation their microstructural features, elemental composition, and hardness were determined by scanning electron microscopy with energy-dispersive X-ray (EDX) microanalysis, X-ray diffraction (XRD) analysis, and Vickers hardness testing. The electrochemical properties were evaluated by anodic potentiodynamic scanning in 0.9% NaCl and Ringer's solutions. Hardness, corrosion current (I_{corr}), and corrosion potential (E_{corr}) were statistically analyzed by one-way analysis of variance and Tukey test ($\alpha = .05$).

Results: EDX analysis showed that all materials belong to the Ag-Zn-Cu ternary system. Three different mean atomic contrast phases were identified for LEO and ORT and two for DEN and NOB. According to XRD analysis, all materials consisted of Ag-rich and Cu-rich face-centered cubic phases. Hardness testing classified the materials in descending order as follows: DEN, 155 ± 3; NOB, 149 ± 3; ORT, 141 ± 4; and LEO, 136 ± 8. Significant differences were found for I_{corr} of NOB in Ringer's solution and E_{corr} of DEN in 0.9% NaCl solution.

Conclusion: Ag-based soldering alloys demonstrate great diversity in their elemental composition, phase size and distribution, hardness, and electrochemical properties. These differences may anticipate variations in their clinical performance. (*Angle Orthod.* 2014;84:508–515.)

KEY WORDS: Soldering; Ag-based alloys; Microstructure; SEM; EDX; XRD; Electrochemical properties

INTRODUCTION

Silver (Ag)-based soldering alloys are extensively used in the manufacturing of orthodontic appliances (brackets, bands with soldered tubes, space maintainers, headgears, orthodontic retainers, hyrax appliances, and others) that join dissimilar stainless steel (SS) alloys. Metallic in nature, with a large surface area exposed to the oral environment, orthodontic appliances are always a concern in the orthodontic literature because of their potential for adverse biological effects due to release of heavy metal ions though corrosion and/or wear mechanisms.[1]

Contemporary Ag-based soldering formulations used for the soldering of custom-made appliances in dental labs are based on the Ag-Zn-Cu ternary system, with small additions of Ni or Sn.[2] To comply with the ISO requirements for Cd-free alloys (a maximum allowable limit for Cd: 0.02% mass fraction),[3] these formulations have been developed to replace the Cd-rich family of Ag-based solders.[4]

---

[a] PhD Graduate Student, Department of Biomaterials, School of Dentistry, National and Kapodistrian University of Athens, Athens, Greece.

[b] Director, Dental Biomaterials Research and Development Chair, Associate Professor, Prosthetic Dental Sciences Department, College of Dentistry, King Saud University, Riyadh, Saudi Arabia.

[c] Director, Dental and Biomaterials Research Group Dental School, "Charite" Medical University of Berlin, Germany.

[d] Professor and Director, Department of Biomaterials, School of Dentistry, National and Kapodistrian University of Athens, Athens, Greece.

[e] Assistant Professor, Department of Biomaterials, School of Dentistry, National and Kapodistrian University of Athens, Athens, Greece, and Consultant, Dental Biomaterials Research and Development Chair, King Saud University, Riyadh, Saudi Arabia.

Corresponding author: Dr Spiros Zinelis, Department of Biomaterials, School of Dentistry, National and Kapodistrian University of Athens, Thivon 2 Str, Goudi 11527, Athens, Greece (e-mail: szinelis@dent.uoa.gr)

Accepted: September 2013. Submitted: July 2013.

DOI: 10.2319/073013-569.1

Table 1. Brand Name, Manufacturer, Elemental Composition, Melting Range, Casting Temperature, and Group Code of Ag Solders Tested, According to Their Manufacturers

Brand Name	Composition, wt%	Melting Range, °C	Casting Temperature, °C	Code
Universal Silver Solder Dentaurum, Ispringen, Germany	Ag: 59, Zn: 25, Cu: 16	N/A	700	DEN
Orthodontic Solders Leone, Florence, Italy	Ag: 55, Zn: 22, Cu: 21, Sn: 2	630–660	N/A	LEO
Ortho Dental Universal Solder Nobil Metal, Villafranca d'Asti, Italy	Ag: 59, Zn: 25, Cu: 16	655–680	700	NOB
Silver Solder Ortho Technology Inc, Tampa, Fla	Ag: 1.5–55, Cu: 19–95, Zn: 2–44, Ni: 0.1–24	>660[a]	N/A	ORT

[a] Melting point.

However, many experimental studies have documented that this system is very prone to decomposition of Cu and Zn,[5–8] a finding which has been recently verified by clinical data.[9,10] The clinical implication of this phenomenon is twofold: First, the joint itself undergoes mechanical degradation,[11,12] which has been associated with early failure of space maintainers.[13–16] Second, and more importantly, there are possible adverse biological consequences—throughout the literature, Ag-based solders demonstrated the worst biocompatibility, showing the greatest reduction in cell proliferation in comparison with other orthodontic metallic materials.[17–20] Excess intake of Zn may cause some functional impairment in the immunological response, limit Fe absorption, and reduce high-density lipoprotein cholesterol, whereas excess Cu uptake has been implicated in liver damage, gastrointestinal irritation, and the neurodegenerative process.[21]

Nevertheless, other researchers[22] do not share the same concerns, claiming that both Cu and Zn belong to nutritionally essential elements needed for bodily functions.[21] Regardless of whether it exceeds the tolerable upper daily intake level, this approach is associated only with acute toxicity and disregards the ability of metal ions to trigger long-term damage associated with subclinical or chronic damage.[10] Furthermore, beyond the adverse effects of diffusion of Cu and Zn in the body, their accumulation at the adjacent tissues has been associated with allergic reaction[23] and oral lesions.[24]

Despite the extensive use of these appliances, especially in children, there is still a lack of information on the microstructural and electrochemical characterization of contemporary dental Ag-based soldering alloys. Such a study could elucidate the in vivo degradation mechanisms involved, since multiphase materials are prone to galvanic corrosion and selective ionic leaching, a mechanism commonly known as dealloying, in which specific elements are selectively dissolved from metallic structures.[25,26] Differences in the elemental composition among contemporary Ag-based solders might affect corrosion resistance and, thus, the clinical efficacy of specific alloys over others.

The aim of the present study was to characterize the microstructure, hardness, and electrochemical behavior of Ag-based soldering alloys. The null hypothesis was that there are no significant differences in these properties among the materials tested.

MATERIALS AND METHODS

Four commercially available Ag-based soldering alloys with indications for soldering orthodontic works were included in this study and are shown in Table 1, along with their nominal elemental composition, melting range, casting temperatures, and group code.

An adequate amount of each alloy was melted in a reducing flame and placed in a mold to fabricate five disk-shaped specimens of each material. For melting LEO and ORT, the corresponding fluxes provided by their manufacturers were used (Leone fluoride flux paste and Ortho Technology TruFlow Orthodontic Flux, respectively), whereas for NOB and DEN the flux was embedded in the structure of the wire as a separate layer. The specimens were conventionally ground with SiC paper up to grit 4000 and polished with a diamond suspension (DiaPro; Struers, Ballerup, Denmark) on both sides.

The specimens were examined with a scanning electron microscope (SEM; Quanta 200; FEI, Hillsboro, Ore) equipped with an energy-dispersive X-ray spectrometer (EDX; Sapphire; EDAX Int, Mahwah, NJ). The microstructural features and elemental composition of the alloys tested were investigated by recording atomic number-contrast backscattered electron images (BE) employing a solid-state detector at a 30-KV accelerating voltage, 108-μm beam current, and 400×, 3200×, and 12000× nominal magnifications. The elemental composition was determined by EDX microanalysis using a liquid N_2-cooled Si detector with a super-ultrathin Be window. Spectra were collected employing an area scan mode (640 × 640-μm sampling area), 300-second acquisition time, and 30%–34% detector dead time. Indicative elemental compositions of different phases based on mean atomic number contrast were determined by spot analysis. The quantitative analysis was performed by Genesis software (version 5.2; EDAX Int) under a nonstandard mode using atomic number-absorption-florescence correction methods.

After SEM-EDX analysis, three specimens from each group were subjected to X-ray diffraction (XRD) analysis (D8 Advance; Bruker, Mass) using a 40-kV accelerating voltage, 40-mA beam current, 30°–110° 2θ-angle scan range, 0.02°/s scanning speed, 0.02° sampling pitch, and 1-second preset time.

The Vickers hardness of the alloys tested was determined in a hardness tester (Diatronic 2Rc; Wolpert, Ludwigshafen, Germany) applying 1 Kp of load and 15 seconds of loading time ($n = 5$).

Electrochemical properties were investigated with anodic potentiodynamic scanning (AS) measurements employing a mini cell system and two different electrolyte solutions. A saturated calomel electrode (SCE; $E_o = 241$ mV vs standard hydrogen electrode) and a Pt wire were used as a reference and an auxiliary electrode, respectively. The assembly was connected to a computer-controlled potentiostat (Voltalab PGZ402; Radiometer Analytical, Villeurbanne Cedex, France), and the electrolyte solutions used were Ringer's (9 g NaCl, 0.24 g $CaCl_2 \cdot 6H_2O$, 0.43 g KCl, and 0.2 g $NaHCO_3$ in 1000 ml distilled water) and NaCl (0.9% wt). AS spectra were acquired at a potential range of -1 V to $+1.25$ V (vs SCE) with a scan rate of 10 mV/s and a 0.008-cm^2 sampling area. Five spectra were collected for each group at ambient temperature, and the corrosion potential E_{corr} and corrosion current I_{corr} were determined after Tafel modeling employing a 200-mV range for cathodic and anodic reactions.

The HV, E_{corr}, and I_{corr} values were statistically analyzed by one-way analysis of variance and multiple-comparison Tukey test at an $\alpha = .05$ level.

RESULTS

Figure 1 shows the BE images at 400× and 3200× nominal magnification, along with inset images (12,000× nominal magnification) for LEO and ORT in Figure 1d,h, respectively. The areas of different phases based on different mean atomic numbers, where spot analysis took place, are also noted on the images with an asterisk as L (low mean atomic number), M (medium mean atomic number), and H (high mean atomic number).

The microstructure of DEN (Figure 1a,b) contains granules with a dendritic structure and needle-like formations within a matrix of a lower mean atomic number. Figure 1c shows the LEO microstructure with a diffuse distribution of higher (white) and lower (black) mean atomic number phases compared to the matrix (gray). LEO (Figure 1d) illustrates that the L (low mean atomic number) is nested in the H (high mean atomic number) phase. NOB shows a microstructure similar to DEN (Figure 1e,f). ORT depicts the diffuse distribution of a lower mean atomic number (Figure 1g), with the matrix consisting of mainly acicular grains (Figure 1h).

In Table 2, the results of the area and EDX analysis are demonstrated. LEO and ORT have lower Ag content compared to NOB and DEN. The latter two alloys have similar compositions. LEO also contains Sn, whereas ORT contains Ni. From the spot analysis, it is documented that DEN and NOB share similar elemental compositions in low and high mean atomic number areas, respectively, with the areas of high mean atomic numbers enriched in Ag content and depleted in Cu and Zn. In LEO, the Ag content increased from low mean atomic number areas toward high ones, whereas Cu and Zn followed an inverse trend. All the aforementioned phases are characterized as Ag-based phases, apart from the low mean atomic number phases of LEO and ORT, which are Cu-based phases.

XRD analysis (Figure 2) showed that all the alloys consist of an Ag-rich face-centered cubic (FCC) and a Cu-Zn FCC phase.

The results of hardness testing (Table 3) indicate that DEN and NOB have the highest hardness, followed by ORT. LEO showed the lowest hardness.

Figure 3 illustrates representative AS curves in a linear and logarithmic scale for the alloys tested in both solutions. The mean values and standard deviations for E_{corr} and I_{corr} are presented in Table 4. The AS in linear scale (Figure 3c,d) showed a pick (hardly visible for LEO, NOB, and ORT) around -100 mV, followed by a limited stability area, with a continuous increase in current toward higher potential for LEO, NOB, and ORT. DEN demonstrated a second pick at about 250–450 mV, followed by a decrease in current in more anodic potentials. Additionally, in the linear scale, NOB seems to reach a "plateau" over the 800 mV.

DISCUSSION

Based on the results of this study, the null hypothesis must be rejected; significant differences were found in the microstructure, hardness, and electrochemical properties of the materials tested. Area scan elemental analysis showed that all the materials belong to the Ag-Zn-Cu system, with LEO and ORT having small additions of Sn and Ni, respectively, which are apparently added to decrease their melting point.[27] LEO and ORT have higher Cu content (Table 2) at the expense of Ag, justifying their

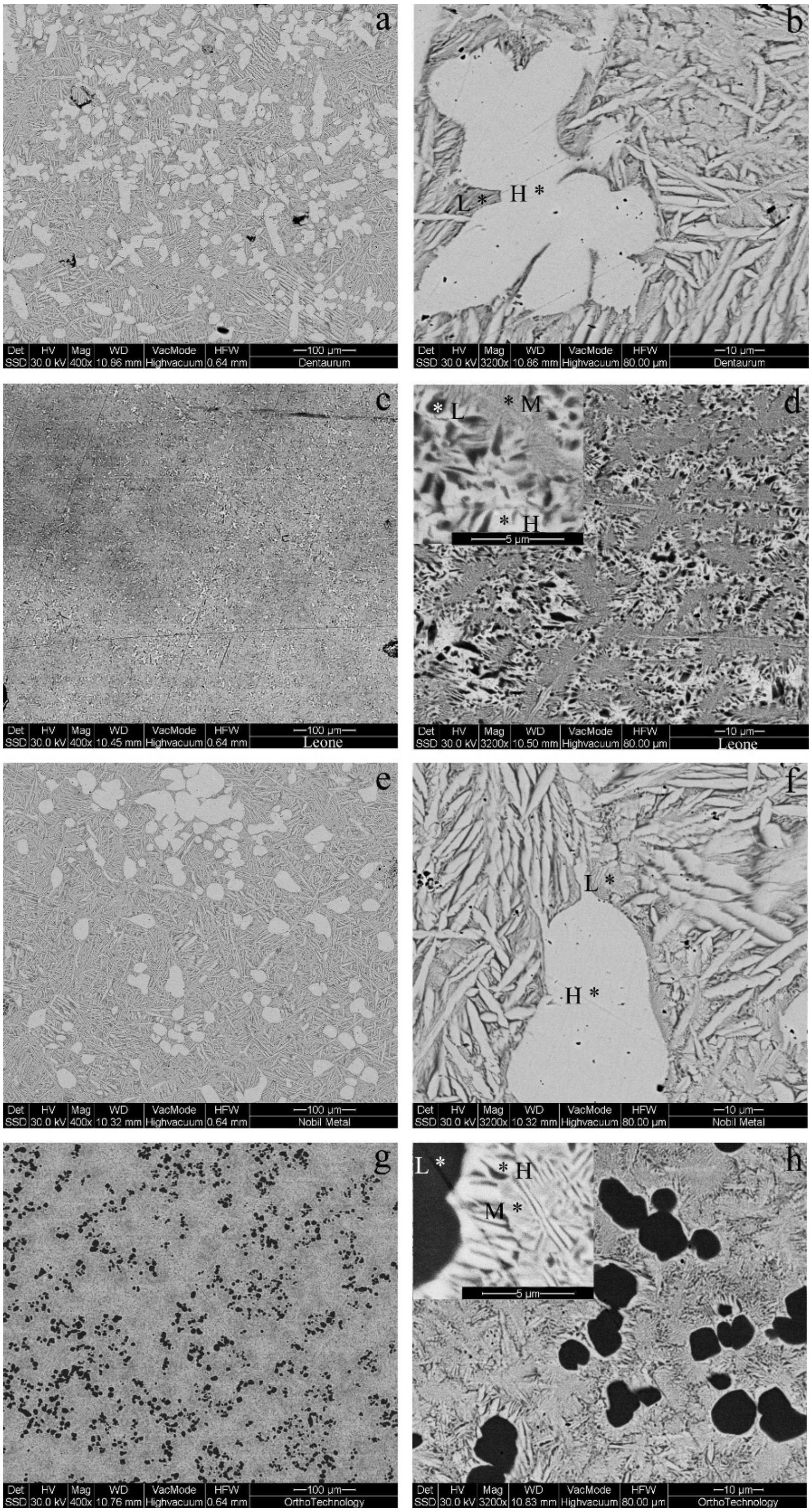

Figure 1. BE images of DEN (a,b), LEO (c,d), NOB (e,f), and ORT (g,h) at 400× (left column) and 3200× (right column) nominal magnification. For LEO and ORT (d and h, respectively), a 12000× nominal magnification image is enclosed. Asterisks indicate the locations of spot analysis.

Table 2. Elemental Composition of the Specimens of the Alloys Tested After Area and Spot EDX Analysis (wt%)[a]

Alloy	Mode	Ag	Zn	Cu	Sn	Ni	O
DEN	Area	61.4	22.4	15.6			0.6
	Spot L	56.6	22.2	20.1			1.1
	Spot H	69.6	18.2	10.6			1.6
LEO	Area	48.8	25.6	23.3	1.9		0.4
	Spot L	10.2	33.4	51.8	3.9		0.7
	Spot M	53.1	22.0	22.6	1.8		0.5
	Spot H	58.3	24.0	13.1	4.1		0.5
NOB	Area	59.4	22.5	16.7			1.4
	Spot L	59.7	20.3	18.8			1.2
	Spot H	69.8	18.6	10.8			0.8
ORT	Area	48.2	26.4	21.1		2.9	1.4
	Spot L	9.1	34.8	43.3		12.2	0.6
	Spot M	52.7	23.2	21.7		1.7	0.7
	Spot H	59.1	23.2	13.7		2.3	1.7

[a] EDX indicates energy-dispersive X-ray; L, low mean atomic number; H, high mean atomic number; and M, medium mean atomic number. See Table 1 for descriptions of the alloy abbreviations.

lower melting points as given by their manufacturers (Table 1).

DEN and NOB have similar two-phase microstructures, whereas LEO and ORT have three different phases. For DEN and NOB microstructures, the dendritic phases should be appended to the formation of the primary Ag-rich solid solution phase, (Ag)FCC, as described by the Ag-Zn-Cu ternary phase diagram,[28] followed by the transformation of acicular or needle-like (Ag)FCCs and Cu-rich solid solution phases, i.e., (Cu)FCCs, at lower temperatures. However, the presence of a Cu-rich phase was not identified (Table 2), probably due to low spatial resolution of EDX analysis compared to the phase size. Nevertheless, the presence of (Cu)FCC was verified in both alloys by XRD analysis (Figure 2). The presence of (Ag)FCC and (Cu)FCC fits well with the Ag-Cu-Zn ternary phase diagram and the elemental ratios of abovementioned alloys as presented in Figure 4. Despite the similarity in their elemental composition, LEO and ORT (Table 2) demonstrated completely different microstructures. LEO showed a diffuse distribution of heavy and light phases (inset Figure 1d). These heavy and light phases are Ag- and Cu- based phases (Table 2) and, thus, should be appended to the (Ag)FCC and (Cu)FCC phases, respectively. ORT illustrates a diffuse distribution of low atomic contrast phase with typical peritectic formation in a lamellar structure. The microstructural differences between ORT and LEO should be attributed to the effect of Sn and Ni in the solidification mechanism, because Sn has limited solubility in Cu in solid phase, whereas Ni is completely soluble in Cu below solidus. The effect of Sn and Ni in the microstructure of Ag-Zn-Cu solders has previously been reported.[27]

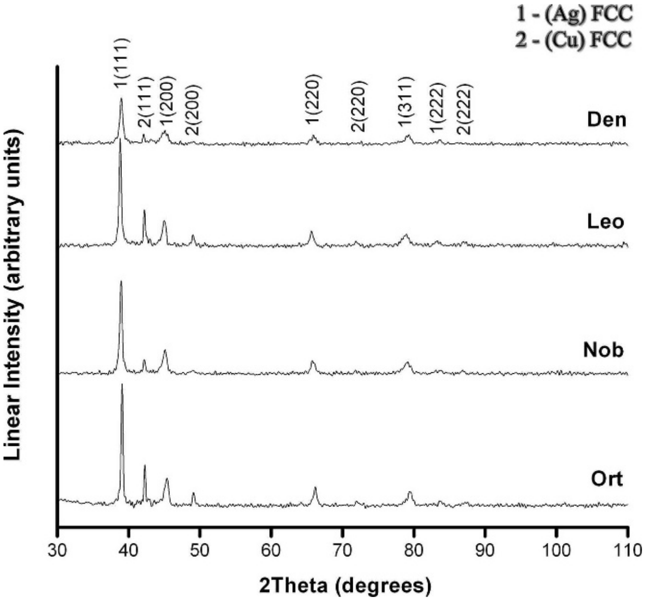

Figure 2. XRD graphs of the alloys tested. 1, Ag-rich matrix (cubic FCC); 2, Cu-rich matrix (cubic FCC).

Ag(FCC) and Cu(FCC) were identified by XRD, and this finding is in agreement with the ternary phase diagram (Figure 4) and previous studies.[27] Although XRD analysis cannot be used for phase quantification, it is interesting that the ratio of Cu primary peak 2(111) to Ag primary peak 1(111) is higher for LEO and ORT

Table 3. Mean Values, Standard Deviations, and Tukey Grouping for Hardness Values of the Alloys Tested*

Alloy	VH
DEN	155 ± 3 ^{a}
LEO	136 ± 8 ^{b}
NOB	149 ± 9 ^{ac}
ORT	141 ± 4 ^{bc}

* VH indicates Vickers hardness test value. See Table 1 for descriptions of the alloy abbreviations. Same alphabetic superscripts denote mean values without statistically significant differences ($P > .05$).

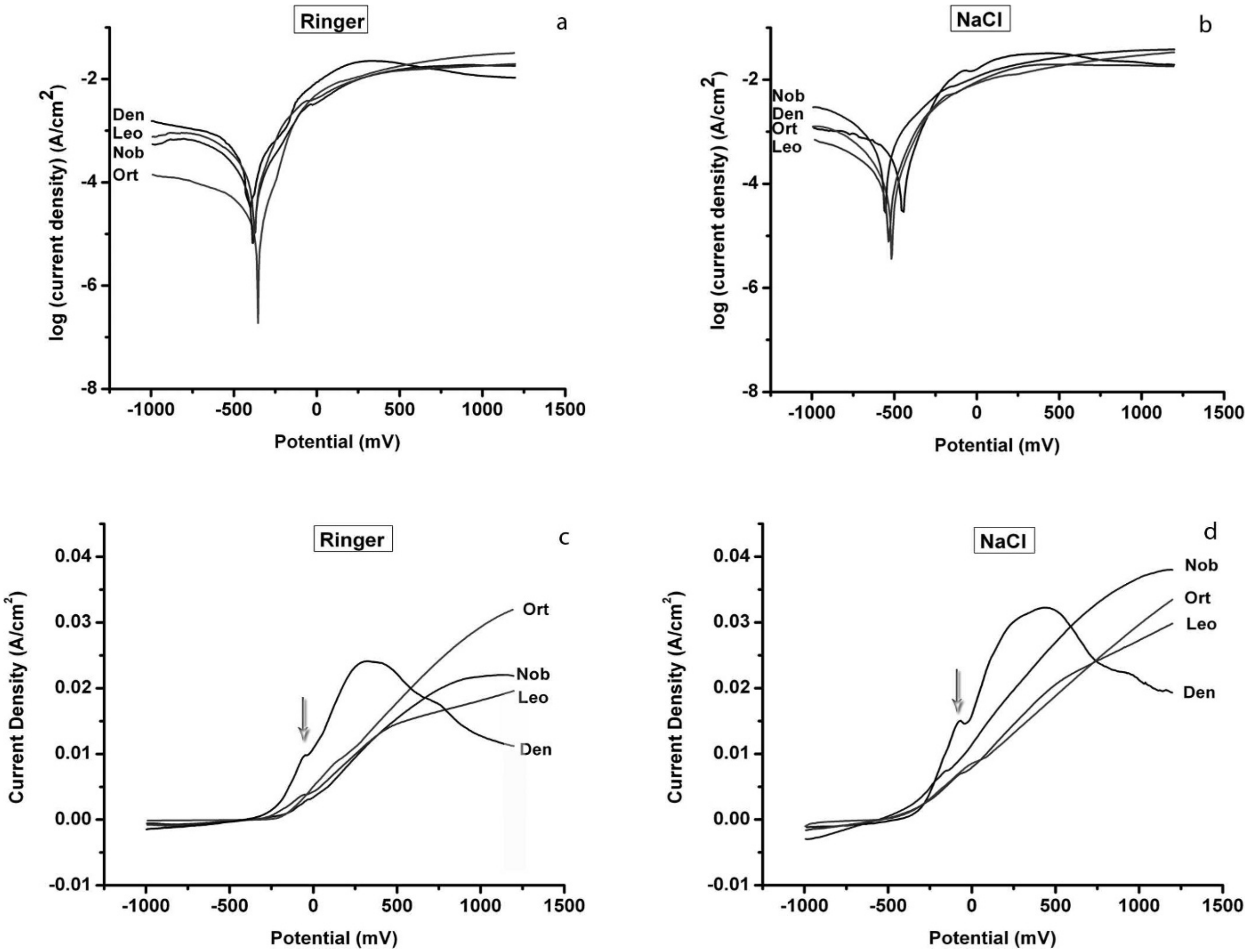

Figure 3. AS curves of the soldering alloys tested in logarithmic (a,b) and linear scale (c,d) for 0.9% NaCl (a,b) and Ringer (c,d) solutions. A local plateau for DEN (but hardly present for the other alloys) at the same region is indicated by the arrows in Ringer (c) and NaCl (d) solutions.

compared to those of DEN and NOB, indicating an increase in volume content of Cu phase exactly the same as that proposed by the relative location of these alloys in the ternary phase diagram (Figure 4) and previous data.[29,30] The higher volume content of the softer Cu phase should explain the lower hardness of LEO and ORT compared to that of DEN and NOB. Further research with advanced analytical techniques (such as transmission electron microscopy-EDX and X-ray Photoelectron Spectroscopy-XPS) can provide substantial information for phase characterization and solidification mechanisms.

In the present study, the lack of statistically significant differences in E_{corr} values of the alloys tested in Ringer's solution denotes similar thermodynamic behavior, whereas the significantly lower I_{corr} of ORT denotes a slower redox reaction rate compared to the other alloys. Furthermore, the E_{corr} values in

Table 4. E_{corr} and I_{corr} Values in Ringer and 0.9% NaCl Solutions for All the Materials Tested*

	Ringer's		0.9% NaCl	
Material	E_{corr}, mV	I_{corr}, A/cm^2	E_{corr}, mV	I_{corr}, A/cm^2
DEN	-397 ± 23 ^{a}	$2.4 \pm 0.2 \times 10^{-4}$ ^{a}	-441 ± 14 ^{a}	$2.9 \pm 0.9 \times 10^{-4}$ ^{a}
LEO	-345 ± 40 ^{a}	$3.5 \pm 2.9 \times 10^{-4}$ ^{a}	-533 ± 6 ^{b}	$1.8 \pm 1.9 \times 10^{-4}$ ^{a}
NOB	-381 ± 7 ^{a}	$1.0 \pm 0.1 \times 10^{-4}$ ^{a}	-558 ± 3 ^{b}	$8.3 \pm 6.5 \times 10^{-4}$ ^{a}
ORT	-342 ± 18 ^{a}	$7.5 \pm 0.3 \times 10^{-6}$ ^{b}	-525 ± 13 ^{b}	$1.2 \pm 0.4 \times 10^{-4}$ ^{a}

* E_{corr} indicates corrosion potential; I_{corr}, corrosion current. See Table 1 for descriptions of the material abbreviations. Same superscripts denote mean values without statistically significant differences ($P > .05$)

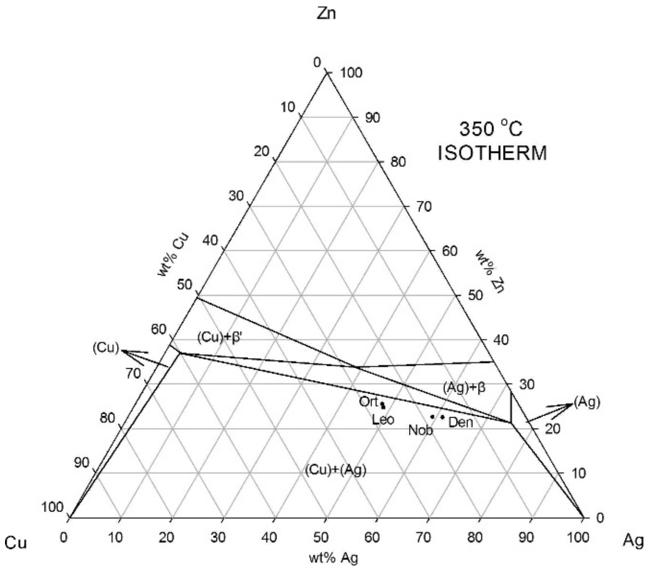

Figure 4. The lower isotherm (350°C) of the Ag-Zn-Cu ternary phase diagram, with black dots indicating the elemental composition of alloys tested. (Ag) and (Cu) stand for Ag-rich and Cu-rich solid solution phases, respectively. Information is missing from the upper part of the diagram.

0.9% NaCl solution are shifted cathodically compared to those in Ringer's solution, probably due to the lower concentration of electrochemically active species in the solution. The significantly higher E_{corr} for DEN in 0.9% NaCl indicates that it is more difficult for this alloy to be oxidized. The fact that the I_{corr} values in the 0.9% NaCl solution do not demonstrate statistical significant differences implies that the kinetics of the redox couples in all the alloys tested are the same.

There are interesting qualitative differences in the voltammograms among the alloys tested, which remained similar in both solutions. The small plateau, identified at approximately −100 mV, can be attributed to Cu oxidation[31] leading to the formation of a protective layer on the surface, which is ruined in slightly higher potentials. The continuously increasing current of LEO, NOB, and ORT denotes that these alloys have passed to the transpassive region. Contrary to LEO and ORT, the increasing current slope is eliminated in NOB approximately above 900 mV, reaching a steady current area, implying a possible second passive region. DEN demonstrated a second wide peak (250–450 mV) followed by a current decrease, indicating surface passivation in both solutions.

Despite the improved electrochemical properties of DEN over the other alloys, recently published retrieval data for DEN and LEO have indicated that both these alloys suffer from decomposition of Cu and Zn in the oral environment.[9] Therefore, similar behavior is anticipated for the remaining alloys based on similarities in elemental composition and structure. Interestingly, the decrease in the Cu content for DEN after intraoral aging of space maintainers was threefold less compared to that of LEO. This may be attributed to the better electrochemical properties and/or decreased Cu content of DEN compared to that of LEO. In addition to this study, it would be interesting to test the galvanic couple of Ag-based soldered alloys with different types of orthodontic wires to identify the least vulnerable combination in galvanic corrosion.

Contemporary Ag-based soldering alloys have complex microstructures, and the presence of (Cu)FCC seems to be the weakest link in this family. Therefore, further research should be done toward Cu replacement in the formulation of these alloys or development of new joining techniques for custom-made orthodontic appliances.

CONCLUSIONS

- All Ag-based soldering alloys tested were based on the Ag-Zn-Cu ternary system.
- Despite great differences in their microstructure, all alloys had Ag and Cu phases.
- DEN was the only alloy with a passive region in both the solutions tested.

ACKNOWLEDGMENT

This study has been funded by a research grant (RGP-VPP-206) from the Research Group Program, Deanship of Scientific Research, King Saud University, Riyadh, Saudi Arabia.

REFERENCES

1. House K, Sernetz F, Dymock D, Sandy JR, Ireland AJ. Corrosion of orthodontic appliances—should we care? *Am J Orthod Dentofacial Orthop*. 2008;133:584–592.
2. Zinelis S, Soteriou S, Ntasi A, Papagianoulis L, Eliades G. Elemental characterization of contemporary Ag-based soldering alloys. Poster presented at: 23rd Congress of the International Association of Paediatric Dentistry; June 15–18, 2011; Athens, Greece.
3. International Organization for Standardization. *Dentistry—Brazing Materials* [ISO 9333:2006]. Geneva: International Organization for Standardization; 2006.
4. Brockhurst PJ, Pham HL. Orthodontic silver brazing alloys. *Aust Orthod J*. 1989;11:96–99.
5. Heidemann J, Witt E, Feeg M, Werz R, Pieger K. Orthodontic soldering techniques: aspects of quality assurance in the dental laboratory. *J Orofac Orthop*. 2002;63:325–338.
6. Mikulewicz M, Chojnacka K. Release of metal ions from orthodontic appliances by in vitro studies: a systematic literature review. *Biol Trace Elem Res*. 2011;139:241–256.
7. Mikulewicz M, Chojnacka K, Wolowiec P. Release of metal ions from fixed orthodontic appliance [published online ahead of print March 11, 2013]. *Angle Orthod*. doi:10.2319/113012-911.1
8. Staffolani N, Damiani F, Lilli C, et al. Ion release from orthodontic appliances. *J Dent*. 1999;27:449–454.

9. Soteriou D, Ntasi A, Papagiannoulis L, Eliades T, Zinelis S. Decomposition of Ag-based soldering alloys used in space maintainers after intra-oral exposure. A retrieval analysis study. *Acta Odontol Scand*. Posted online on July 4, 2013. (doi:10.3109/00016357.2013.812745).
10. Freitas MP, Oshima HM, Menezes LM. Release of toxic ions from silver solder used in orthodontics: an in-situ evaluation. *Am J Orthod Dentofacial Orthop*. 2011;140:177–181.
11. Vahed A, Lachman N, Knutsen RD. Failure investigation of soldered stainless steel orthodontic appliances exposed to artificial saliva. *Dent Mater*. 2007;23:855–861.
12. Bock JJ, Bailly J, Gernhardt CR, Fuhrmann RA. Fracture strength of different soldered and welded orthodontic joining configurations with and without filling material. *J Appl Oral Sci*. 2008;16:328–335.
13. Qudeimat MA, Fayle SA. The longevity of space maintainers: a retrospective study. *Pediatr Dent*. 1998;20:267–272.
14. Rajab LD. Clinical performance and survival of space maintainers: evaluation over a period of 5 years. *ASDC J Dent Child*. 2002;69:156–160.
15. Tulunoglu O, Ulusu T, Genc Y. An evaluation of survival of space maintainers: a six-year follow-up study. *J Contemp Dent Pract*. 2005;6:74–84.
16. Baroni C, Franchini A, Rimondini L. Survival of different types of space maintainers. *J Pediatr Dent*. 1994;16: 360–361.
17. Freitas MP, Oshima HM, Menezes LM, Machado DC, Viezzer C. Cytotoxicity of silver solder employed in orthodontics. *Angle Orthod*. 2009;79:939–944.
18. Berge M, Gjerdet NR, Erichsen ES. Corrosion of silver soldered orthodontic wires. *Acta Odontol Scand*. 1982;40: 75–79.
19. Grimsdottir MR, Hensten-Pettersen A, Kullmann A. Cytotoxic effect of orthodontic appliances. *Eur J Orthod*. 1992; 14:47–53.
20. Mockers O, Deroze D, Camps J. Cytotoxicity of orthodontic bands, brackets and archwires in vitro. *Dent Mater*. 2002;18: 311–317.
21. Food and Nutrition Board. Dietary Reference Intakes for Vitamin A, Vitamin K, Arsenic, Boron, Chromium, Copper, Iodine, Iron, Manganese, Molybdenum, Nickel, Silicon, Vanadium, and Zinc. Washington, DC: National Academic Press, 2000:224–252, 442–489.
22. Zahrowski JJ. Silver solder toxicity? Show me the evidence. *Am J Orthod Dentofacial Orthop*. 2012;140:756–757. Author reply 757–758.
23. Schuster G, Reichle R, Bauer RR, Schopf PM. Allergies induced by orthodontic alloys: incidence and impact on treatment. Results of a survey in private orthodontic offices in the Federal State of Hesse, Germany. *J Orofac Orthop*. 2004;65:48–59.
24. Bishara SE. Oral lesions caused by an orthodontic retainer: a case report. *Am J Orthod Dentofacial Orthop*. 1995;108: 115–117.
25. Sun D, Monaghan P, Brantley WA, Johnston WM. Electrochemical impedance spectroscopy study of high-palladium dental alloys. Part II: behavior at active and passive potentials. *J Mater Sci Mater Med*. 2002;13:443–448.
26. Sarkar NK, Berzins DW, Prasad A. Dealloying and electroformation in high-Pd dental alloys. *Dent Mater*. 2000;16: 374–379.
27. Zhongmin L, Songbai X, Xianpeng H, Liyong G, Wenhua G. Study on microstructure and property of brazed joint of AgCuZn-X(Ga, Sn, In, Ni) brazing alloy. *Rare Metal Mater Eng*. 2010;39:397–400.
28. Chang YA, Goldberg D, Neumann JP. Phase diagrams and thermodynamic properties of ternary copper-silver systems. *J Phys Chem Ref Data*. 1997;6:621–673.
29. Warinsiriruk E, Phung-on I. Microstructure of induction brazed interface between cobalt-based alloy and martensitic stainless steel using Ag-Cu-Zn filler metal. *Asian Int J Sci Technol Prod Manuf Eng*. 2010;3:41–44.
30. Yoo YC, Kim JH, Park K. Microstructural characterization of Al2O3/AISI 8650 steel joint brazed with Ag-Cu-Sn-Zr alloy. *Mater Lett*. 2000;42:362–366.
31. Mueller WD, Schoepf C, Nascimento ML, et al. Electrochemical characterisation of dental alloys: its possibilities and limitations. *Anal Bioanal Chem*. 2005;381:1520–1525.